Nitric Oxide 87 (2019) 1–9

Contents lists available at ScienceDirect

Nitric Oxide

journal homepage: www.elsevier.com/locate/yniox

Sodium/calcium exchanger is involved in apoptosis induced by H_2S in tumor cells through decreased levels of intracellular pH

Ivan Szadvari[a], Sona Hudecova[b], Barbora Chovancova[b], Miroslava Matuskova[c], Dana Cholujova[c], Lubomira Lencesova[b], David Valerian[a], Karol Ondrias[b], Petr Babula[a,d], Olga Krizanova[a,b,*]

[a] Department of Physiology, Faculty of Medicine, Masaryk University, Brno, Czech Republic
[b] Institute of Clinical and Translational Research, Biomedical Research Center, Slovak Academy of Sciences, Bratislava, Slovakia
[c] Cancer Research Institute, Biomedical Research Center, Slovak Academy of Sciences, Bratislava, Slovakia
[d] International Clinical Research Center, St. Anne's University Hospital Brno, Brno, Czech Republic

ARTICLE INFO

Keywords:
Apoptosis
Hydrogen sulfide
Intracellular acidification
Sodium/calcium exchanger
Sodium/hydrogen exchanger

ABSTRACT

We explored possibility that sodium/calcium exchanger 1 (NCX1) is involved in pH modulation and apoptosis induction in GYY4137 treated cells. We have shown that although 10 days treatment with GYY4137 did not significantly decreased volume of tumors induced by colorectal cancer DLD1 cells in nude mice, it already induced apoptosis in these tumors. Treatment of DLD1 and ovarian cancer A2780 cells with GYY4137 resulted in intracellular acidification in a concentration-dependent manner. We observed increased mRNA and protein expression of both, NCX1 and sodium/hydrogen exchanger 1 (NHE1) in DLD1-induced tumors from GYY4137-treated mice. NCX1 was coupled with NHE1 in A2780 and DLD1 cells and this complex partially disintegrated after GYY4137 treatment. We proposed that intracellular acidification is due to uncoupling of NCX1/NHE1 complex rather than blocking of the reverse mode of NCX1, probably due to internalization of NHE1. Results might contribute to understanding molecular mechanism of H_2S–induced apoptosis in tumor cells.

1. Introduction

Role of the hydrogen sulfide (H_2S) in a variety of physiological/pathophysiological processes has already been described. Among these, involvement of the H_2S in apoptosis induction in cancer cells was described in several papers [1–3], although targeting of different pathways was proposed. H_2S overdrives cancer glycolysis and at the same time impairs the activity of pH regulators, anion exchangers and sodium/proton exchanger (NHE1). Consequently, such combined effects warrant H_2S to enhance lactate production and shut down cancer cell capacity to regulate its pH homeostasis. Together, H_2S brings about cancer cell death via intracellular acidification [4,5].

Sodium/hydrogen exchangers (NHE) belong to potent proton extrusion transport systems. NHEs family is a group of membrane proteins that transport one H^+ out of cells in exchange for one Na^+ into cells. Nine NHE isoforms (NHE1-9) have been identified up to now. The type 1 NHE (NHE1) is an integral membrane transport protein involved in regulating pH and in tumor cells is a major contributor to the production and maintenance of their reversed proton gradient and thus an important regulator of both pHi and pHe in tumors [6]. NHE1 is quiescent at physiological pHi (pHi ≥ 7.2), but its activity increases rapidly upon intracellular acidification [7]. During intracellular acidification, allosteric modification at the proton binding site led to stimulation of NHE1 activity. Activation of a variety of cell surface receptors can regulate the activity of NHE1 by modulating the *C*-terminal tail region [8,9]. It was reported that H_2S could decrease activities of both the anion exchanger and the sodium/proton exchanger, but has no effect on the expression levels of pH regulators [5]. The enhanced metabolic acid production and defective pH regulation together cause an uncontrolled intracellular acidification, thereby resulting in cancer cell death [10].

To avoid the overload of cancer cells by sodium, sodium/calcium exchanger (NCX) can switch to the reverse mode and extrude excess of sodium out of cells. It was already shown that the NCX operates in reverse mode in some cancer cells [11–13]. NCX is also one of key players in the regulation of an intracellular calcium homeostasis. Three types of the NCX were found and characterized up to now; however, type 1 NCX (NCX1) is the most abundant and therefore best studied type. Although majority of papers dealing with the NCX1 originates from the cardiac tissue [14,15], importance of this calcium transporter

* Corresponding author. Institute of Clinical and Translational Research, Biomedical Research Center, Slovak Academy of Sciences, Dubravska cesta 9, 84505, Bratislava, Slovakia.
E-mail address: olga.krizanova@savba.sk (O. Krizanova).

https://doi.org/10.1016/j.niox.2019.02.011
Received 5 November 2018; Received in revised form 31 January 2019; Accepted 28 February 2019
Available online 05 March 2019

was documented also in other types of cells and tissues, where it can be involved in apoptosis and regulation of cell proliferation [16]. It was already shown that NCX can play a role also in the apoptosis development [17,18]. We have already shown that sulfide signaling induced by GYY4137 (a slow-releasing H_2S donor) treatment is involved in regulation of the NCX1 and apoptosis induction *in vitro* [3].

It is widely accepted that increased glycolytic potential is one of the hallmarks of cancer. Malignant cells have at least 20- to 30-fold higher rate of glycolysis than normal cells, mainly due to switch in enzyme's complex changes in the glycolytic pathway [19]. Treatment with 400 μM GYY4137 for 5 days significantly increases glycolysis and results in excess lactate production in MCF7 and HepG2 cancer cells [10]. Specific genes and signaling molecules involved in the tumor-forced glycolysis and related phenomena, such as pH regulation, may represent potential therapeutic targets of agents that specifically interact with the key factors of tumor phenotype. Thus, a novel practical strategy that regulates cancer cell pH could be an effective approach to induce cancer cell death [20]. The enhanced metabolic acid production and defective pH regulation together can cause an uncontrolled intracellular acidification, thereby resulting in cancer cell death. Given the natural differences in the acid metabolism of cancer and normal cells, low and continuous exposure to H_2S may serve as a novel and effective strategy in eliminating cancer cells without harming normal cells [10]. We proposed that mechanism of H_2S-induced apoptosis can act also through the hyper-acidification of the intracellular space. Therefore, in this work we explored possibility that the type 1 sodium/calcium exchanger is involved in pH modulation in GYY4137 treated cells resulting in apoptosis induction. We also explored possibility of the interaction and/or mutual communication of the NCX1 and NHE1 in the intracellular acidification.

2. Material and methods

2.1. Cell cultivation, treatment and proliferation

For experiments, ovarian cancer cell line A2780 (Sigma-Aldrich, 93112519), colon adenocarcinoma cell line DLD1 (ATCC, CCL-221) and endothelial EA.hy926 cell line (ATCC® CRL-2922TM) was cultured in Dulbecco Minimal Essential Medium (DMEM; Sigma, USA) or RPMI medium (Sigma, USA) with a high glucose (4.5 g/L) and L-glutamine (300 μg/ml), supplemented with 10% fetal bovine serum (Sigma, USA), penicillin (Calbiochem, USA; 100 U/mL) and streptomycin (Calbiochem, USA; 100 μg/mL). Cells were cultured in a water-saturated atmosphere at 37 °C and 5% CO_2. After plating, cells were treated with GYY4137 (1, 10, 100 and 1000 μmol/L), or KB-R7943 mesylate (KBR; Santa Cruz Biotechnology; 10 μmol/L; blocker of the NCX1 reverse mode) for 24 h. Proliferation of DLD1/A2780 cells was determined in IncuCyte Live Cell Analysis System (Essen Bioscience) on 96-well plate using 1000/2000 cells per well. Proliferation was evaluated for the period of 7 days.

2.2. Detection of apoptosis with Annexin-V-FLUOS

After the GYY4137 treatment, DLD1 cells were gently scraped and pelleted at 1000 × *g* for 5 min. Cells were then washed with 1 ml of PBS (phosphate saline buffer pH 7.4), pellet was resuspended in 200 μl of Annexin-V-FLUOS/propidium iodide labeling solution (Roche Diagnostics, USA) and incubated at room temperature for 20 min in dark according the manufacturer's protocol. After the incubation, samples were diluted with 400 μl of PBS, placed on ice and measured on BD FACSCanto II flow cytometer (Becton Dickinson, Ann Arbor, USA).

2.3. Measurement of intracellular pH

Changes in intracellular pH (pHi) were measured by pH sensitive cell permeable fluorescent probe 2′,7′–biscarboxyethyl–5,6–carboxyfluorescein - acetoxymethyl ester (BCECF-AM; Sigma Aldrich, USA) as described in Pastorek et al. [21]. Cells plated onto 24-well plates were loaded with 10 μmol/L BCECF and 0.5% pluronate in cultivation media without FBS for 45 min at 37 °C, 5% CO_2, in dark. Afterwards, cells were washed twice with PBS buffer and fluorescence was measured at 490/535 nm and 440/535 nm on Synergy fluorescence scanner (BioTek, Germany). The pHi signal was calibrated to pH0 by adding 10 μmol/L nigericin (Sigma Aldrich, USA) with 130 mmol/L KCl. ΔpHi was calculated in ratiometric manner from values obtained at 490 and 440/535 nm.

2.4. In vivo experiments on nude mice

All animal experiments were approved by the Committee on the Protection of Animals, Faculty of Medicine, Masaryk University, and performed according to the institutional guidelines and the European Community Guide for the Care and Use of Laboratory Animals.

DLD-1 cells (5×10^6 cells) resuspended in 0.1 ml PBS were injected subcutaneously (s.c.) into the flank of 4- to 5-week-old male athymic nude mice under a light anesthesia (xylazine 10 mg/kg). Visible tumors developed after 3 days. Mice were then randomly divided into either a treatment group (20 or 50 mg/kg GYY4137 diluted in 0.5% carboxymethylcellulose (CMC), given daily as an oral gavage), or a control group (0.5% CMC). Tumors were measured every 3 days with a caliper, and the tumor volume (V) was calculated according to the formula: $V = \text{length} \times (\text{width})^2$, the width being the greatest transverse diameter and length the greatest longitudinal diameter. Mice were kept on standard pelleted food and water *ad libitum*, monitored daily for the weight loss or other signs of possible toxic effects of the drug.

After 10 or 13 days (20 mg/kg or 50 mg/kg, respectively) of therapy, nude mice were deeply anesthetized (ketamine, xylazine) and sacrificed. Tumors were resected, weighed and cryopreserved at −80 °C for further experiments. The effect of GYY4137 on tumor growth was evaluated by comparing the tumor volume and/or weight of the treated and control groups.

2.5. TUNEL assay

Tissue sections (5 μm in thickness) were prepared from the tumor samples from nude mice, and stained using Fluorescein *in situ* cell death detection kit (Roche, Germany) according to the standard protocol provided by the manufacturer (Roche 11684795910, version 17). Nuclei were counterstained using Hoechst 33285 solution (0.5 μg/ml, 14530, Sigma-Aldrich, USA). Sections were visualized by epi-fluorescence microscopy using Nikon Eclipse Ti−S/L100 (Nikon, Japan); NIS elements software (Nikon, Japan) was used to evaluate the images. Quantification of the signal was performed as a ratio of Fluorescein-dUTP to Hoechst 33258 signal.

2.6. Immunohistochemistry (IHC)

IHC staining of the tumor tissue sections (5 μm in thickness) was conducted according to the standardized protocols provided by Abcam (www.abcam.com). Following primary antibodies were used: rabbit anti-Na^+/Ca^{2+} exchanger (Swant, Switzerland) diluted 1:5000 and monoclonal Anti-SLC9A1 diluted 1:100. Consequently, sections were stained with FITC-labeled secondary antibodies using goat anti-rabbit (F9887, Sigma-Aldrich, USA) or anti-mouse (ab96879, Abcam, UK) IgG diluted 1:500 or 1:750, respectively. Both primary and secondary antibodies were diluted in 1% BSA in TBS. The nuclei staining and processing of images were performed as described above.

2.7. Isolation of RNA and real-time PCR

Total RNAs was isolated from tumors induced by DLD1 cells in nude mice by TRI Reagent (Sigma, USA) as described in Novotna et al. [22]. The purity and integrity of isolated RNAs were checked on GeneQuant

Pro spectrophotometer (Amersham Biosciences, UK). Reverse transcription was performed using 1.5 μg of total RNAs and Ready-To-Go You-Prime First-Strand Beads with the pd(N6) primer (GE Healthcare Life Sciences, UK). The real-time PCR amplification and detection was carried out on the Applied Biosystems StepOneTM RealTime PCR Systems (Applied Biosystems, USA) as described in Chovancova et al. [23]. The expression of target genes - NCX1 and NHE1 was normalized to the expression of housekeeping gene β-actin. For detection of the β-actin, NCX1 and NHE1 following primers were designed: human β-actin: 5′- ACA TCT GCT GGA AGG TGG AC- 3' (forward); 5′- TCC TCC CTG GAG AAG AGC TA - 3' (reverse); human NCX1: 5′- TCC CAT CTG TGT TGT GTT CGC - 3' (forward); 5′- TCA TCT TGG TCC CTC TCA TC - 3' (reverse); human NHE1: 5′- TAG GGT TAG TTC TGG AGC TGG A- 3' (forward); 5′- TGA GAT TCC GGG GAA ATG GAA - 3' (reverse). Melting analysis was performed after each run of real-time PCR.

2.8. Isolation of proteins, western blot analysis and immunoprecipitation

After GYY4137 treatment cells were trypsinized and resuspended in distilled water. Afterwards, homogenates were centrifuged for 1 h at 100 000 × *g* (rotor Type 70.1Ti, Beckman Coulter Optima™ L-100K Ultracentrifuge; Beckman Coulter, California, USA). Cytosolic proteins occurred in supernatant and membrane proteins were found in pellet. Protein concentration of the homogenate, membrane fraction and supernatant were determined by using the method of Lowry et al. [24]. Whole procedure is described in detail in Lencesova et al. [25]. For immunoprecipitation, appropriate monoclonal antibodies (3 μg) or polyclonal antibodies (~6 μg) were incubated with ~2×10^7 (50 μl) washed magnetic beads (Dynabeads M-280); coated with goat anti-mouse IgG or M-280 sheep anti-rabbit IgG; (Invitrogen Dynal AS, Norway) for overnight at 4 °C on a rotator (VWR International). As negative controls, beads were incubated with mouse IgG1κ (MOPC-21; Sigma, USA). The beads with attached antibody were washed (twice, 200 μl) with phosphate buffered saline (PBS). Proteins were immunoprecipitated from 1 mg of detergent-extracted total protein by incubation for 4 h at 4 °C with antibody-bound beads. Following incubation, the supernatant was frozen and later used for immunoblotting. Bead complexes were washed with (four times 200 μl) PTA (1,45 M NaCl, 0,1 M NaH2PO4, 0,1 M sodium azide, and 0.5% Tween 20, pH 7.0). Immunoprecipitated proteins were then extracted with 60 μl of 2 × sodium dodecyl sulfate (SDS) sample buffer (0.5 M Tris, 10% SDS, glycerol, bromphenol blue, DTT) and boiled for 5 min. An enhanced chemiluminescence detection system (LuminataTM Crescendo Western HRP Substrate, Millipore) was used to detect the bound antibodies. To detect NCX1, NHE1 and clathrin proteins, a rabbit polyclonal antibody NCX1 (120 kDa, π11-13, Swant, Switzerland), rabbit polyclonal NHE1 antibody (91 kDa, ab67314, Abcam, UK) and rabbit polyclonal clathrin antibody (180 kDa, ab21679, Abcam, UK) were used. As a housekeeper, we used β-actin mouse monoclonal [AC-15] antibody (42 kDa, ab6276, Abcam, UK).

2.9. Proximity ligation assay

Proximity ligation assay (PLA) was used to study the interaction between NCX1/NHE1. The assay was performed in a humid chamber at 37 °C according to the manufacturer's instructions (Olink Bioscience, Sweden). A2780 and/or DLD1 cells were seeded on glass cover slips and allowed to attach before treatment with GYY4137 for 24 h. Afterwards, the cells were fixed with methanol, blocked with 3% BSA/PBS for 30 min, incubated with a mixture of antibodies against NCX1 and NHE1 for 1 h, washed three times, and incubated with plus and minus PLA probes for 1 h. Then, the cells were washed (3 × 5 min), incubated for 40 min with ligation mixture containing connector oligonucleotides, washed again, and incubated with amplification mixture containing fluorescently labeled DNA probe for 100 min. After a final wash, the samples were mounted and the signal representing interaction between NCX1 and NHE1 was determined by confocal microscope imaging system TCS SPE-II (Leica, Wetzlar, Germany) with 405-nm and 532-nm lasers for excitation. To measure the intensity of fluorescence, software - LAS AF (Leica Application Software platform for confocal microscope) was used. Rabbit polyclonal antibody NCX1 (π11-13, Swant, Switzerland) and mouse monoclonal NHE1 (SLC9A1, Sigma-Aldrich, USA) were used in the experiment.

2.10. Determination of cell cycle

Changes in cell cycle were determined by flow cytometric measurement of DNA content of nuclei labeled with propidium iodide (PI). Briefly, cells (3×10^5) were collected using cell scrapper, washed twice with cold PBS and incubated in 300 μl PBS with 0.05% Triton X-100 and 15 μl RNA-se A (10 mg/ml) for 20 min at 37 °C. Afterwards, cells were cooled on ice for at least 10 min before PI (50 μg/ml) was added. Finally, the stained cells were analyzed using a FACS Aria II flow cytometer (Becton Dickinson) equipped with 488 nm excitation laser and filters for cell cycle analysis: log 675/40 - sub-G0; lin 585/42 - DNA cell cycle histogram; (585/42 peak area vs. peak hight for doublets discrimination). Forward/side light scatter characteristic was used to exclude the cell debris from the analysis. For each sample, 1×10^4 cells were acquired and analyzed with De Novo FCS Express software (De Novo software, Los Angeles, CA, USA).

2.11. Cytosolic $[Ca^{2+}]i$ staining by Fura2-AM fluorescent dye

Cells were plated on a 24-well plate at the density of 4×10^4. After treatment, the cells were washed with 1 ml of serum-free medium and loaded with 20 μM FURA-2 AM; (Sigma-Aldrich, USA) in the presence of 0.5% pluronate (Sigma-Aldrich,USA) and 0.1 nM ionomycine in serum-free medium for 40 min at 37 °C in the dark. The cells were then washed three times with a 500 μl of phosphate saline buffer (PBS). Fluorescence was measured on the fluorescence scanner Synergy II (BioTek, Germany) at λex 340/380 nm and λem 516 nm. The results were calculated as ratio between 340 and 380 nm and expressed as relative fluorescence units (RFU).

2.12. Cytosolic $[Na^+]i$ staining by SBFI-AM fluorescent dye

Intracellular concentration of sodium $[Na^+]i$ was measured according to Sathish et al. [26] with some modifications. Briefly, cells were loaded with 5 μmol/L SBFI-AM in the presence of 0.1% of pluronate, 10 μmol/L gramicidin and 100 μmol/L ouabain in the serum free DMEM for 3 h in CO_2 incubator. Afterwards, cells were washed twice with 5% glucose. Excitation was measured at 340 and 380 nm and emission at 500 nm. Results were expressed as ratio between these two values.

2.13. Immunofluorescence

Cells grown on glass coverslips were fixed in ice-cold methanol. Non-specific binding was blocked by incubation with PBS containing 3% bovine serum albumin (BSA) for 60 min at a room temperature. Cells were then incubated with primary antibody - mouse monoclonal NHE1 (SLC9A1, Sigma-Aldrich, USA, dilution 1:100) - diluted PBS with 1% BSA (PBS-BSA) for 1 h at 37 °C. Afterwards, cells were washed three times with PBS-BSA for 10 min, incubated with CF Fluor® 488 or CF Fluor® 594 goat anti-rabbit (or anti-mouse) IgG diluted 1:1000 in PBS-BSA for 1 h at 37 °C, and washed as described previously. Finally, coverslips were mounted onto slides in mounting medium Fluoroshield with DAPI (F6057, Sigma). Images of all samples were acquired with the same microscope setup. Cells were visualized by epifluorescence microscopy using Nikon Eclipse Ti−S/L100 (Nikon, Japan); NIS elements software (Nikon, Japan) was used to process images and to evaluate the resultant pictures.

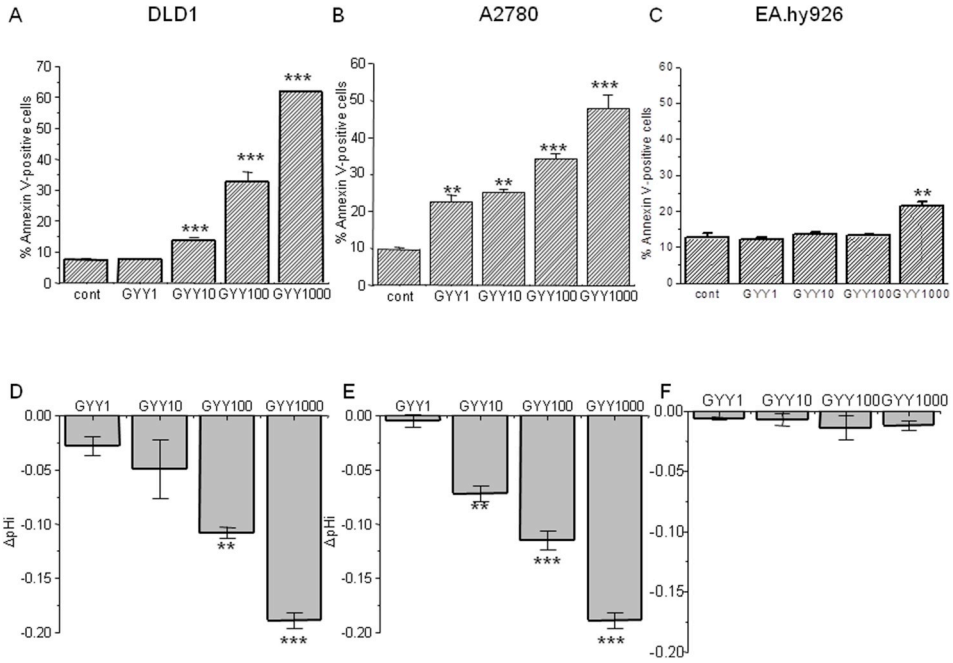

Fig. 1. Concentration-dependent effect of the GYY4137 on apoptosis induction and intracellular pH in DLD1 (A, D), A2780 (B, E) and EA.Hy926 (C, F) cells. Apoptosis was detected by Annexin V-FLUOS in cells treated with 1 μmol/L, 10 μmol/L, 100 μmol/L and 1000 μmol/L GYY4137 for 24 h (A, B, C). As expected, concentration-dependent increase in apoptosis due to GYY4137 treatment was observed in DLD1 and A2780 tumor cells (A, B), but not in non-tumor endothelial cell line EA.hy926 (C). Also, intracellular pH decreased when DLD1 and A2780 cells were treated with 1 μmol/L, 10 μmol/L, 100 μmol/L and 1000 μmol/L GYY4137 for 24 h (D, E). In EA.hy926 cells, no changes in the intracellular pH were observed after GYY4137 treatment (F). Each column is displayed as mean ± S.E.M and represents an average of three independent cultivations, each performed in triplicates. Statistical significance ** compared to corresponding control represents $p < 0.01$ and ***$p < 0.001$.

2.14. Statistical analysis

Each value represents an average of 3–6 wells from at least two independent cultivations of DLD1 and/or A2780 cells. Results are presented as mean ± S.E.M. Significant differences between the groups were determined by one-way ANOVA. For multiple comparisons, an adjusted *t*-test with p values corrected by the Bonferroni method was used.

3. Results

3.1. Concentration-dependent effect of slow sulfide donor GYY4137 on apoptosis induction and intracellular acidification

Slow sulfide donor GYY4137 induced apoptosis in a concentration-dependent manner in DLD1 (Fig. 1A) and A2780 (Fig. 1B) cells, but not in endothelial EA.Hy926 cells (Fig. 1C). Concentration of 1 μmol/L did not induce apoptosis in DLD1 cells. Concentration of 1 mmol/L GYY4137 was too high, since majority of the DLD1 and A2780 cells were apoptotic. EA.Hy926 cells were not affected by GYY4137 treatment, except of concentration of 1 mmol/L, where a slight apoptosis was detected. Also, due to GYY4137 treatment, intracellular acidification occurred in DLD1 and A2780 cells in a concentration-dependent manner (Fig. 1D and E), while no changes in the intracellular pH due to GYY4137 treatment were detected in EA.Hy926 cells (Fig. 1F).

3.2. Effect of GYY4137 on tumor growth and apoptosis induction in nude mice

In nude mice, where tumors were induced subcutaneously using 5×10^6 DLD1 cells, treatment with GYY4137 did not significantly suppress the tumor growth after 10–13 days of treatment (Fig. 2A and B). This time period was chosen based on the work Lu et al. [2], since we were interested in the early processes that affect the tumor growth due to GYY4137 treatment. We observed that tumors from mice treated with GYY4137 (20 mg/kg or 50 mg/kg) were already apoptotic (Fig. 2C and D), as determined by TUNEL assay on tumor slices. Quantification of immunohistochemistry was performed as a ratio of Fluorescein-dUTP/Hoechst 33285 signal (D).

3.3. Changes in expression of NCX1 and NHE1 in tumors from control and GYY4137 treated nude mice

In tumors, NHE1 is known to be involved in regulation of intracellular pH [6] and structural interaction of NHE1 and NCX1 was already suggested [38]. Therefore, we determined levels of NHE1 and NCX1 in tumors induced in control and GYY4137-treated (50 mg/kg, 10–13 days) nude mice by immunohistochemistry (Fig. 3A and B) and also corresponding mRNA levels by real-time PCR (Fig. 3C). Quantification of IHC was performed as a ratio of FITC/DAPI signal (B). We have found increased signal of both NCX1 and NHE1 by immunohistochemistry and also increased levels of NCX1 and NHE1 mRNA in tumors of nude mice treated with GYY4137, compared to tumors from non-treated mice (Fig. 3A,B,C).

3.4. Formation of NCX1/NHE1 complexes studied by proximity ligation assay (PLA) and immunoprecipitation

PLA revealed a complex formation between NCX1 and NHE1 in A2780 and DLD1 cells (Fig. 4A, cont). Number of complexes rapidly decreased due to GYY4137 treatment (10 μmol/L, 24 h) in DLD1 and/or A2780 cells (Fig. 4A, GYY). Decrease in the number of NCX1/NHE1 complexes was not caused by lower expression of these transporters, since both, NHE1 and NCX1 proteins increased due to GYY4137 treatment in DLD1 and A2780 cells (Fig. 4B). As a loading control, β-actin was determined as well (Fig. 4B). The complex formation was verified also by immunoprecipitation with NCX1 in A2780 cells (Fig. 4C).

3.5. Effect of GYY4137 on cell proliferation and changes in cell cycle

Treatment with GYY4137 (10, 100 and 1000 μmol/L, 24 h) resulted in significantly decreased proliferation of DLD1 (10 μmol/L GYY4137 $p = 0.0363$, 100 μmol/L GYY4137 $p = 0.0103$ and 1000 μmol/L GYY4137 $p < 0.0001$) and A2780 cells (10 μmol/L GYY4137 $p = 0.0069$, 100 μmol/L GYY4137 $p = 0.0021$ and 1000 μmol/L GYY4137 $p < 0.0001$) in a concentration-dependent manner (Fig. 4D). Highest concentration of GYY4137 used (1000 μmol/L) resulted in rapid decrease of viability. Determination of cell cycle in DLD1 cells resulted in decrease of number of cells in G2 phase and increase in S

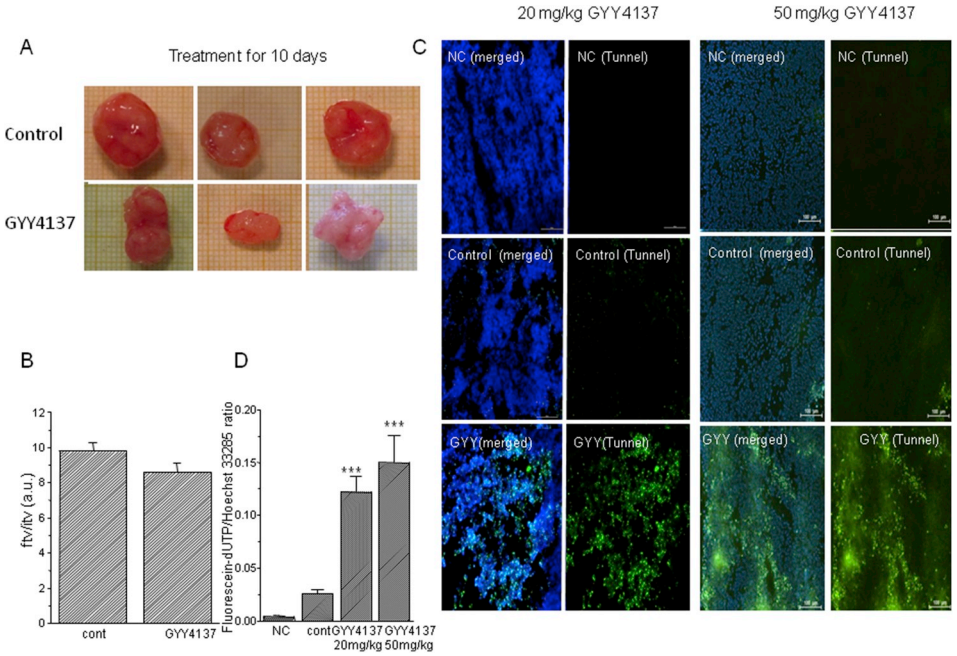

Fig. 2. Effect of GYY4137 on tumor growth in nude mice. Nude Nu/Nu mice were injected by 5×10^6 DLD1 cells s.c. Palpable tumors developed within 3 days. Afterwards, mice were treated with either 0.5% carboxymethyl cellulose alone or with GYY4137 (GYY; 20 or 50 mg/kg) for 10 or 13 days, respectively. Tumors were withdrawn (A) and ratio of final tumor volume (ftv) determined at the day of extirpation and initial tumor volume (itv) determined at the beginning of treatment was calculated (B). Tumors were cut to slices and TUNEL assay was performed (C, D) to determine apoptosis. Hoechst 33258 (blue color) stained nuclei, TUNEL positive cells were stained by Fluorescein (green color) to show DNA fragmentation (C). Fluorescein signal was evaluated relatively to Hoechst 33258 in order to quantify the apoptosis (D). TUNEL assay on tumor slices revealed apoptosis in tumors from mice treated with GYY4137. Columns are displayed as mean ± S.E.M and represent an average of at least five independent measurements. Statistical significance *** compared to corresponding control represents $p < 0.0001$.

phase after GYY4137 treatment (Fig. 4E). In normal non-cancerous epithelial EA.Hy926 cells, no changes were determined in control and GYY4137-treated cells (Fig. 4E). Representative histograms of each group from flow cytometer are also shown (Fig. 4E, inset).

3.6. Changes in cytosolic calcium and cytosolic sodium in DLD1, A2780 and EA.Hy926 cells due to GYY4137 treatment

Further, we tested whether intracellular acidification by GYY4137 can be due to blocking reverse mode of the NCX1. Therefore, we used KB-R7943 (KBR) - a selective blocker of the activity of NCX1 through the reverse mode – and determined levels of cytosolic calcium (Fig. 5A) and cytosolic sodium (Fig. 5B) in DLD1 (black column), A2780 (gray columns) and EA.Hy926 (white columns) cells due to GYY4137 treatment. In these cells, GYY4137 treatment (10 μmol/L) increased cytosolic calcium and did not change levels of cytosolic sodium compared to untreated cells, suggesting that NCX1 still operates in a reverse mode. This suggestion was supported by the observation that KB-R7943 treatment had no effect on levels of cytosolic calcium – they were not changed compared to controls (Fig. 5A), while levels of cytosolic sodium were increased (Fig. 5B). Based on these results we elaborate a hypothesis (Fig. 5C), which will be explained in the section Discussion.

3.7. Internalization of the NHE1

Further, we focused on determination of the possible internalization of NHE1 due to GYY4137 treatment (Fig. 6). From A2780/DLD1 cells we isolated membrane and also cytosolic fraction by ultracentrifugation and determined protein levels of NHE1 and clathrin (a protein, deeply involved in endocytosis; Fig. 6A,B,C). We observed significant changes in NHE1 and clathrin in membrane (memb) and membrane fraction (memb) due to GYY4137 treatment in both types of cells. Also, we observed significantly higher levels of both these proteins in cytosolic fraction (sup). Typical gels of these results are shown in Fig. 6A.

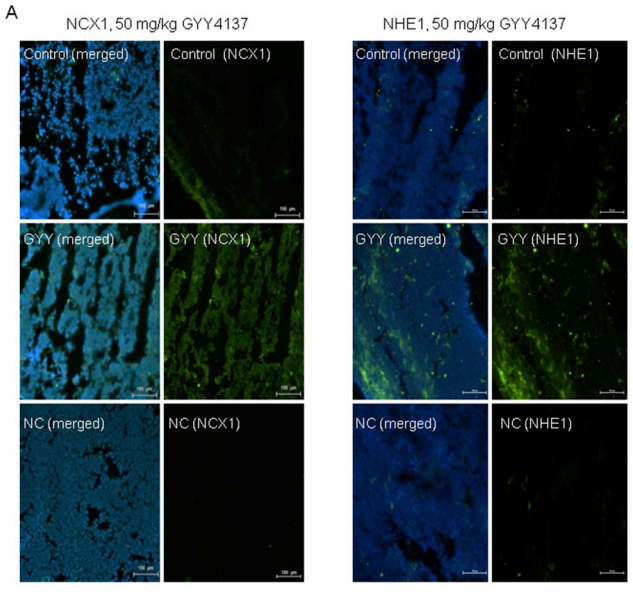

Fig. 3. Determination of the NCX1 and NHE1 by immunohistochemistry (A,B) and real time PCR (C). In tumor slices, increased NCX1 staining was observed in GYY4137 treated mice (GYY; 50 mg/kg), compared to tumor slices from untreated mice (A,B). NC– negative control, where primary antibody was omitted. Quantification of IHC was performed as a ratio of FITC/DAPI signal (B). In tumors from GYY4137 treated mice (GYY; 20 and 50 mg/kg), increased mRNA levels of NCX1 and NHE1 were determined compared to tumors from non-treated mice (C). Each column is displayed as mean ± S.E.M, n = 6. Statistical significance *compared to corresponding control represents $p < 0.05$, **$p < 0.01$ and ***$p < 0.0001$.

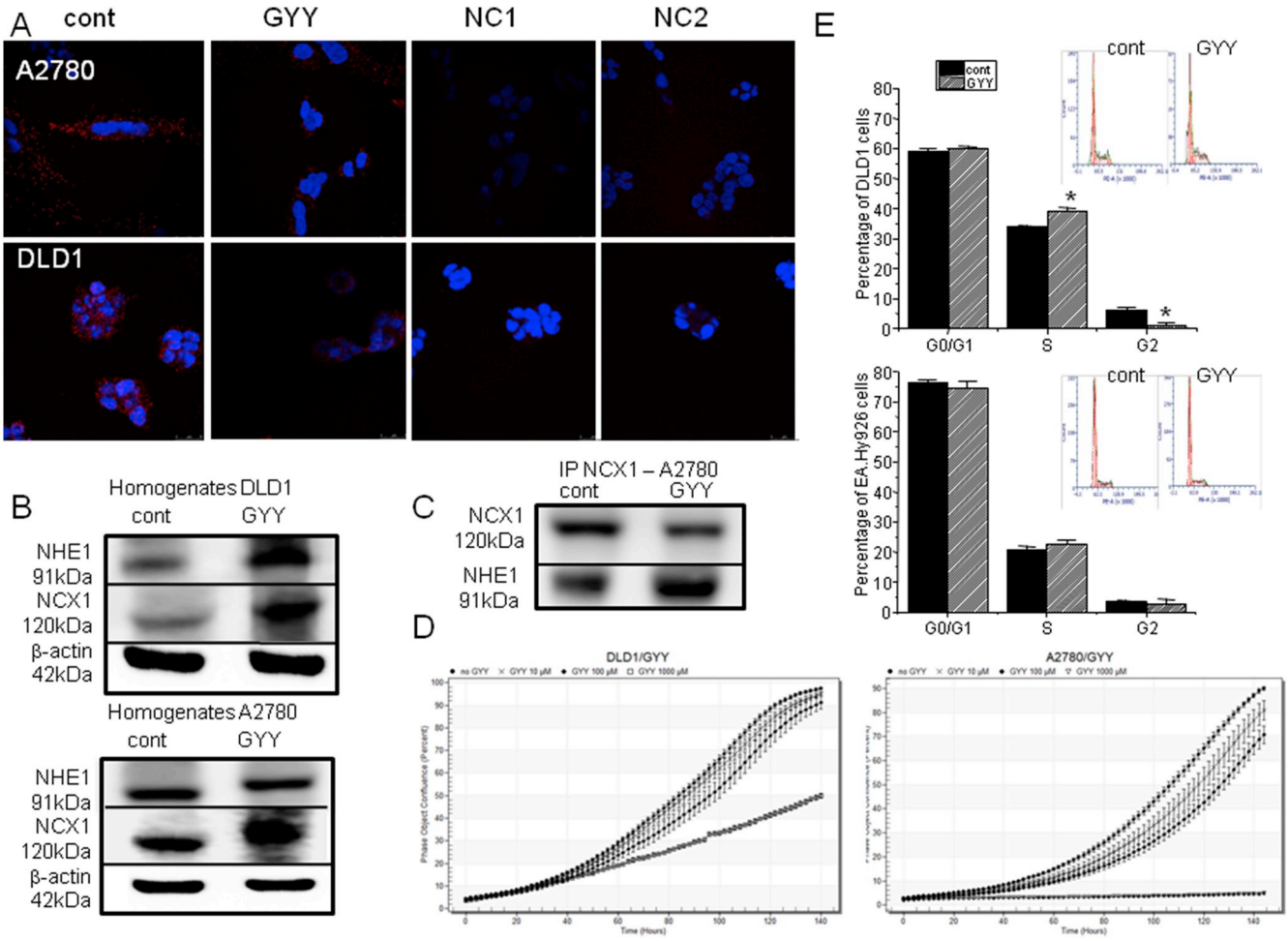

Fig. 4. Effect of GYY4137 (10 μg/L; 24 hrs) treatment on NCX1/NHE1 complex formation (A,B,C), proliferation (D) and cell cycle (E). Proximity ligation assay (PLA; A) of the NCX1 and NHE1 in untreated DLD1 and A2780 cells revealed clear co-localization of the NCX1 and NHE1 (red dots). After the GYY4137 treatment, number of red signal dots was significantly lower, thus suggesting uncoupling of the NCX1 and NHE1 (A). cont – control untreated group, GYY – group treated with GYY4137, NC1 – negative control, where primary antibody against NCX1 was omitted, NC2 – negative control, where primary antibody against NHE1 was omitted. Quantity of NCX1 and NHE1 proteins was verified by Western blot analysis (B). Complex formation was verified by immunoprecipitation with NCX1 antibody on A2780 cells (C). Treatment of DLD1 and A2780 cells with different concentrations of GYY4137 revealed concentration-dependent decrease in their proliferation (D). Determination of the cell cycle showed significant differences in S and G2 phase in DLD1 cells, but not in EA.Hy926 cells after GYY4137 treatment (E). Typical histograms from the flow cytometry are shown in (E). Results in part E are displayed as mean ± S.E.M and represent an average of at least three independent measurements. Statistical significance * compared to corresponding control represents $p < 0.05$.

Immunofluorescence of the NHE1 in control and GYY4137 treated DLD1 cells revealed differences in fluorescence (Fig. 6D). While in control DLD1 cells the signal was sharper and localized mainly on plasma membrane, in GYY4137 treated group the NHE1 signal was more diffused, thus suggesting localization in both, plasma membrane and cytoplasm (Fig. 6D).Co-localization of NHE1 (Fig. 6E, green signal) with clathrin (red signal) in the cytosol after GYY4137 treatment (10 mmol/L, 34 h) is in line with our proposal of GYY4137-induced NHE1 internalization.

4. Discussion

GYY4137 was reported to release H_2S slowly and steadily, either in aqueous solution or administered to the animal [9]. Moreover, it was already confirmed that GYY4137 is a suitable molecule for studying physiological and pathophysiological mechanisms *in vivo* because of its low toxicity [39]. We have shown that GYY4137 was able to induce apoptosis in A2780 and DLD1 tumor cells in a concentration-dependent manner, probably via intracellular hyper-acidification. Several papers reported that H_2S can exhibit or potentiate antimetastatic and/or proapoptotic effects in tumor cells [27–29]. We tested also induction of apoptosis on non-cancerous normal epithelial cells EA.Hy926 and we observed very slight apoptosis induction only at a very high concentration of GYY4137. Thus, we conclude that GYY4137 might be effective in apoptosis induction only in tumor cells. These results are in accordance with Lee et al. [4], who proved that non-cancerous cells exposed to GYY4137 displayed no significant difference in lactate production or intracellular pH in contrast to cancerous cell lines that exhibited both increased lactate production and intracellular acidification after the same treatment.

We have shown that GYY4137 decreased proliferation in a concentration-dependent manner and affects tumor growth when tumor cells are injected subcutaneously to nude mice. Lu et al. [2] injected 5×10^6 liver hepatocellular carcinoma HepG2 cells into nude mice, and after 21–28 days significant difference in tumor size occurred between control and GYY4137-treated mice. However, it is obvious that tumors after 28 days are structurally and metabolically different compared to tumors grown for 10–13 days. Since the aim of our work was to evaluate mechanisms induced by GYY4137 on tumor growth, we selected shorter interval (10–13 days), where tumors in GYY4137 treated mice already started to be smaller than those in control mice, but still the difference was not significant. We injected the same amount of

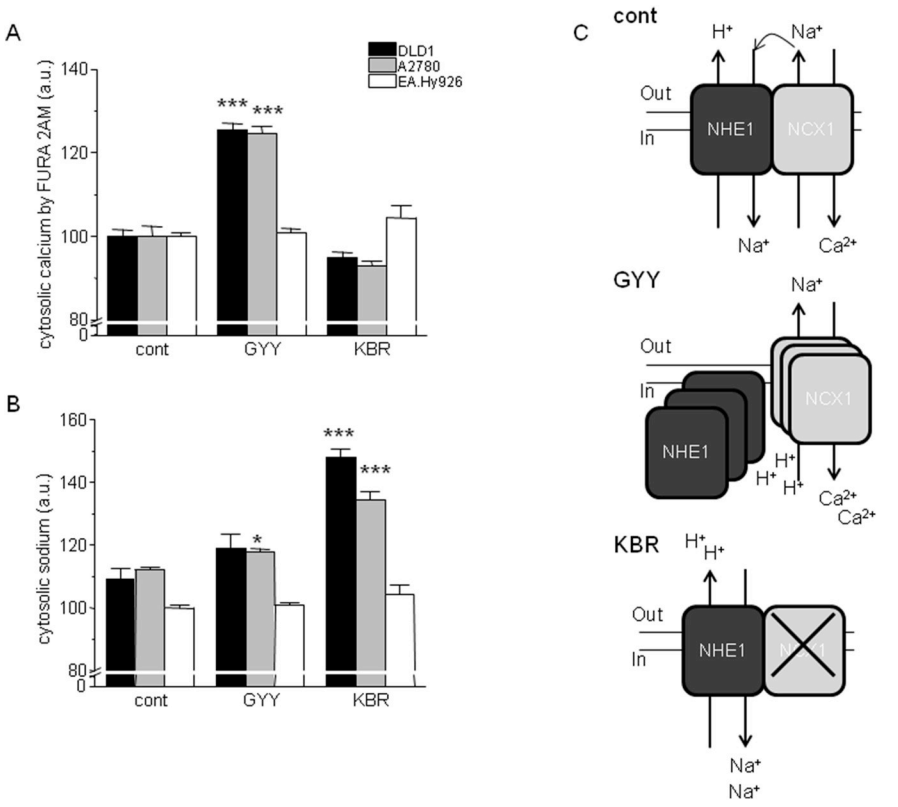

Fig. 5. Levels of cytosolic calcium (A) and cytosolic sodium (B) in DLD1 (black columns), A2780 (gray columns) and EA.Hy926 (white columns) cells. Treatment with GYY4137 (GYY) increased significantly levels of calcium in both, A2780 and DLD1 cells, but did not change cytosolic calcium levels in normal non-cancer EA.Hy926 cells. Selective blocker of the reverse mode NCX1 – KB-R7943 (KBR) – did not significantly change levels of the cytosolic calcium in A2780, DLD1 or EA.Hy926 cells compared to corresponding untreated controls (A). Levels of the cytosolic sodium were increased in group of cells treated with KBR, but not GYY4137 in A2780 and DLD1 cells (B). Also, these levels were not affected by GYY4137 treatment in EA.Hy926 cells (B). Based on the levels of intracellular calcium and sodium, a hypothetic cartoon of the mechanism of action of GYY4137 on cancer cells is shown (C). Each column is displayed as mean ± S.E.M, n = 3–6. Statistical significance * compared to corresponding control represents $p < 0.05$ and ***$p < 0.001$.

DLD1 cells into nude mice and after 10–13 days mice treated with GYY4137 developed tumors that were apoptotic, although the size of these tumors was not significantly different from tumors of untreated mice. These results clearly confirm the ability of GYY4137 to induce apoptosis in tumor cells.

Moreover, we observed concentration-dependent intracellular acidification in DLD1 and A2780 cells treated with GYY4137. The rate of H_2S release from GYY4137 (1 mmol/L, i.e. 100 nmol incubated) was reported to be 4.17 ± 0.5 nmol/25 min, i.e. ~4%/25 min. When incubated in aqueous buffer (pH 7.4, 37 °C), H_2S release sustained over 75 min and after administration (intravenous or intraperitoneal) of GYY4137 to anesthetized rats, plasma H_2S (defined as H_2S, HS^-, and S^{2-}) concentration was increased at 30 min and remained elevated over the 180 min [9]. From these reported results we might estimate that in our study the free concentration of H_2S released from GYY4137 was < 1 μmol/L and this might be similar to the *in situ* physiological concentrations. Lee et al. [5] also observed intracellular hyper-acidification due to GYY4137, but in a concentration of GYY4137 10-40-

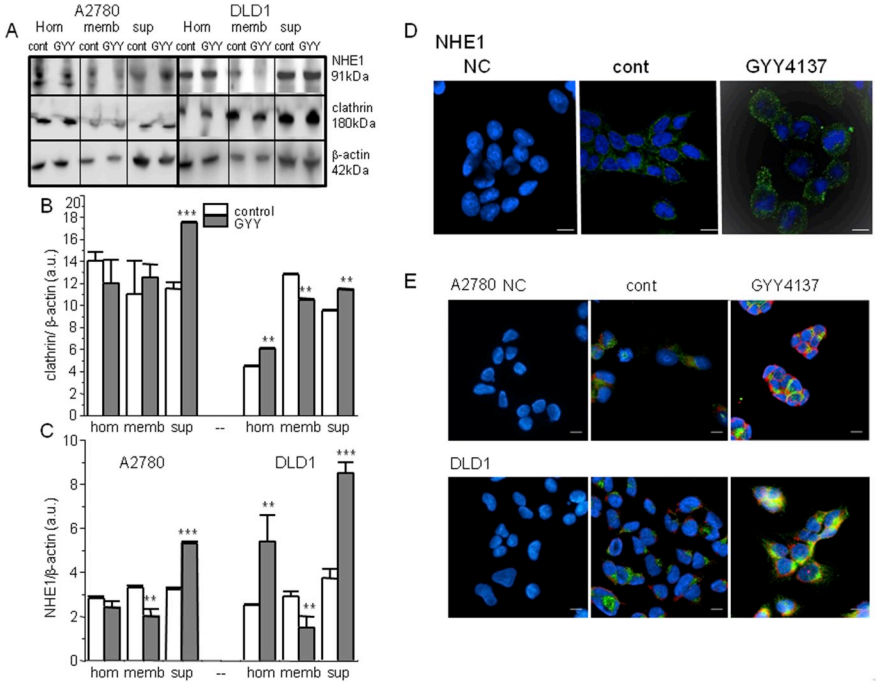

Fig. 6. Internalization of the NHE1 in A2780/DLD1 cells. NHE1 protein (A, C) and also clathrin protein (A, B) was determined in cell's homogenate (hom), membrane fraction (memb) and supernatant (sup). Importantly, levels of both proteins were significantly increased in supernatant fraction of these proteins, while in pellet decreased amounts were observed (A, B, C). Typical gels of NHE1, clathrin and a housekeeper β-actin are shown (A). In NHE1 gel, upper ban corresponds to NHE1 and lower band to proton antiporter 1 transporter, which has a sequence similarity to NHE1, as mentioned in data sheet by antibody provider. When NHE1 was determined by immunofluorescence, NHE1 signal was detectable on the plasma membrane in control cells, while in GYY4137 treated cells, internalization of the signal into the cytoplasm occur (D). Double labeling of A2780 and DLD1 cells with clathrin (green) and NHE1 (red) antibodies also showed internalization of NHE1 into the cells (E). NC– negative control, where primary antibody was omitted; cont – control, untreated cells; GYY4137 – cells treated with GYY44137 for 24 h. Scale bar represents 7.5 μM. Each column is displayed as mean ± S.E.M, n = 3. Statistical significance * compared to corresponding control ***$p < 0.001$.

times higher.

We performed *in vitro* experiments also with endothelial cell line EA.hy926, and proved that apoptosis was slightly induced only when 1 mmol/L GYY4137 was used. Also, an intracelllular pH decrease was not observed in contrast to the cancer cells after the same treatment. Similar outcomes were seen in other studies with no toxicity observed in *in vitro* experiments with GYY4137 using normal or non-cancerous cells lines, such as vascular smooth muscle cells, human non-cancer fibroblasts or hepatocellular cells whereas survival of various cancer cell lines was significantly reduced with the same concentrations applied [2,4,9]. In addition, Lee et al. also proved that non-cancer cells exposed to GYY4137 displayed no significant difference in lactate production or intracellular pH in contrast to cancerous cell lines that exhibited both increased lactate production and intracellular acidification after the same treatment [4].

Acidification is a common feature of tumor cells, because of a bulk lactate production due to anaerobic conditions [19,30]. To compensate the inefficient extraction of energy from glucose and to maintain the biomass production, malignant cells have at least a 20- to 30-fold higher rate of glycolysis than normal cells [31]. Thus, malignant cells accumulate protons and intracellular pH becomes acidic. To prevent hyper-acidification of the intracellular space, variety of proton transporters are activated to extrude protons from the cells. Among them, sodium-proton exchanger of type 1 (NHE1) is of a special interest [32]. The NHE1 is a member of family of integral membrane secondary active acid extruders that mediate the electroneutral 1:1 exchange of extracellular sodium for intracellular protons across the cell membrane. Through its action the inwardly directed sodium gradient can drive the uphill extrusion of protons that alkalinizes pHi and acidifies pHe (for review see Reshkin et al. [6]). In order to prevent overload with Na^+, transport extrusion system is needed to extrude Na^+ ions from the cells. In cancer cells NCX1 works in a reverse mode and therefore serves as a potent extrusion system of Na^+ [3]. In tumors from mice treated with GYY4137, both NCX1 and NHE were increased on mRNA and protein levels.

Using proximity ligation assay we have clearly shown, that NHE1/NCX1 complex is partially disintegrated in DLD1 and also in A2780 cells. Based on these observations we proposed that hyper-acidification in tumor cells observed after GYY4137 treatment might be due to dysregulation of the NHE1/NCX1 complex, rather than due to down-regulation of their expression. Further, we hypothesized that disintegration of the NHE1/NCX1 complex might be either due to switch of the reverse mode NCX1 to forward mode, or due to internalization of the NHE1. Therefore, we compared levels of cytosolic calcium and cytosolic sodium in control, GYY4137 and KB-R7943 treated cells. KB-R7943 is a potent blocker of the reverse mode NCX1 [33]. As expected, in DLD1 and A2780 cells treatment with KB-R7943 resulted in increased levels of cytosolic sodium and no changes in cytosolic calcium compared to control group of cells. On the contrary, treatment with GYY4137 increased level of cytosolic calcium and did not change levels of cytosolic sodium, which shows that during GYY4137 treatment NCX1 works in the reverse mode. Also, as we have shown earlier [3], GYY4137 treatment resulted in a nice NCX1 signal on plasma membrane and no translocation was observed.

It was already reported that slow H_2S-releasing donor, GYY4137, significantly increased glycolysis, leading to overproduction of lactate and intracellular acidification in cancer cells. Also, H_2S decreased anion exchanger and sodium/proton exchanger activity [4]. We proposed that due to GYY4137 treatment NHE1 is not only uncoupled from the NCX1, but also internalized, which might result in the loss of function and accumulation of protons in the cytosol that causes hyper-acidification and induction of apoptosis. Our immunofluorescence results show internalization of the NHE1 into the cytoplasm, thus supporting our proposal.

The NHE1 inhibition due to different reasons has fatal consequences for the cancer cells. Decreasing NHE1 expression or inhibiting its activity leads to hyper-acidification of the intracellular space, inhibition of glycolysis, tumor cell growth arrest and selective apoptosis [34–36]. Lee et al. [5] shown that GYY4137 and simvastatin or metformin synergize to induce intracellular hyper-acidification-mediated cancer cell death. We have shown that GYY4137-induced intracellular hyper-acidification is due to internalization of NHE1 into the cytosol, a process, which inactivates the NHE1. Signal for this process is uncoupling of NHE1 from the NCX1.

Up to now, nothing is known about the effect of H_2S on clathrin-dependent endocytosis. Nevertheless, involvement of H_2S in the process of endocytosis was already shown by Ge et al. [37], who showed that in renal tubular epithelial cells, H_2S can regulate endocytosis of a functional membrane protein, Na^+/K^+- ATPase. H_2S directly targets some disulfide bonds in epidermal growth factor receptor (EGFR), which activates the EGFR/gab1/PI3K/Akt pathway and subsequent Na^+/K^+-ATPase endocytosis and inhibition in renal tubular epithelial cells [37]. Thus, H_2S-induced endocytosis might be another mechanism with important physiological consequence, since clathrin-mediated endocytosis constitutes the major pathway for uptake of signaling receptors into eukaryotic cells. Nevertheless, further studies are required to clarify this issue.

In summary, we have shown that in DLD1 and A2780 cells, NHE1 and NCX1 form conjugates and these complexes are partially disrupted due to GYY4137 treatment leading to the intracellular acidification. H_2S-induced disruption of NHE1/NCX1 complex is associated with overexpression of these proteins and internalization of NHE1. Both proteins participate in the apoptosis induction. The results contribute to understanding of how the NHE1/NCX1 complex is involved in intracellular acidification and apoptosis induction in cancer.

Conflict of interest

All authors have nothing to disclose.

Author's contribution

IS, and DV performed experiments on nude mice and immunohistochemistry, SH performed Annexin V-FLUOS assay, pH measurements and determination of intracellular sodium and calcium, MM performed proliferation assays, DCH did cell cycle experiments, LL performed proximity ligation assay and Western blot analysis, BCH performed immunofluorescence, viability and molecular biology experiments, KO and PB participate on manuscript writing, OK conceived and designed the study and was in charge for manuscript preparation. All authors read and approved the final manuscript.

Funding

This work was supported by grant APVV-16-0246, APVV-14-0351, VEGA 2/0073/16, LQ1605 (MEYS CR, NPU II) and MUNI/A/1255/2018.

Acknowledgement

Authors wish to thank to Mrs. Marta Sirova for an excellent technical assistance. The study was also supported by the Research and Development Operational Programme funded by the European Regional Development Fund ITMS: 26240220044. Authors would like to acknowledge Dr. Roller with the PLA imaging on confocal microscope.

References

[1] K. Kashfi, Anti-cancer activity of new designer hydrogen sulfide-donating hybrids, Antioxidants Redox Signal. 20 (5) (2014) 831–846.
[2] S. Lu, Y. Gao, X. Huang, X. Wang, GYY4137, a hydrogen sulfide (H_2S) donor, shows

potent anti-hepatocellular carcinoma activity through blocking the STAT3 pathway, Int. J. Oncol. 44 (4) (2014) 1259–1267.
[3] J. Markova, S. Hudecova, A. Soltysova, M. Sirova, L. Csaderova, L. Lencesova, K. Ondrias, O. Krizanova, Sodium/calcium exchanger is upregulated by sulfide signaling, forms complex with the β1 and β3 but not β2 adrenergic receptors, and induces apoptosis, Pflügers Archiv 466 (7) (2014) 1329–1342.
[4] Z.W. Lee, X.Y. Teo, E.Y. Tay, C.H. Tan, T. Hagen, P.K. Moore, L.W. Deng, Utilizing hydrogen sulfide as a novel anti-cancer agent by targeting cancer glycolysis and pH imbalance, Br. J. Pharmacol. 171 (18) (2014) 4322–4336.
[5] Z.W. Lee, X.Y. Teo, Z.J. Song, D.S. Nin, W. Novera, B.A. Choo, B.W. Dymock, P.K. Moore, R.Y. Huang, L.W. Deng, Intracellular hyper-acidification potentiated by hydrogen sulfide mediates invasive and therapy resistant cancer cell death, Front. Pharmacol. 8 (2017) 763.
[6] S.J. Reshkin, R.A. Cardone, S. Harguindey, Na^+-H^+ exchanger, pH regulation and cancer, Recent Pat. Anti-Cancer Drug Discov. 8 (1) (2013) 85–99.
[7] J. Lacroix, M. Poet, C. Maehrel, L. Counillon, A mechanism for the activation of the Na/H exchanger NHE-1 by cytoplasmic acidification and mitogens, EMBO Rep. 5 (1) (2004) 91–96.
[8] X. Li, J. Ding, Y. Liu, B.J. Brix, L. Fliegel, Functional analysis of acidic amino acids in the cytosolic tail of the Na^+/H^+ exchanger, Biochemistry 43 (51) (2004) 16477–16486.
[9] L. Li, M. Whiteman, Y.Y. Guan, K.L. Neo, Y. Cheng, S.W. Lee, Y. Zhao, R. Baskar, C.H. Tan, P.K. Moore, Characterization of a novel, water-soluble sulfide-releasing molecule (GYY4137): new insights into the biology of hydrogen sulfide, Circulation 117 (2008) 2351–2360.
[10] D. Wu, W. Si, M. Wang, S. Lv, A. Ji, Y. Li, Hydrogen sulfide in cancer: friend or foe? Nitric Oxide 50 (2015) 38–45.
[11] M. Song, D. Chen, S.P. Yu, The TRPC channel blocker SKF 96365 inhibits glioblastoma cell growth by enhancing reverse mode of the Na^+/Ca^{2+} exchanger and increasing intracellular Ca^{2+}, Br. J. Pharmacol. 171 (14) (2014) 3432–3447.
[12] S.R. Sennoune, J.M. Santos, F. Hussain, R. Martínez-Zaguilán, Sodium calcium exchanger operates in the reverse mode in metastatic human melanoma cells, Cell. Mol. Biol. (Noisy-le-grand) 61 (7) (2015) 40–49.
[13] Z. Long, B. Chen, Q. Liu, J. Zhao, Z. Yang, X. Dong, L. Xia, S. Huang, X. Hu, B. Song, L. Li, The reverse-mode NCX1 activity inhibitor KB-R7943 promotes prostate cancer cell death by activating the JNK pathway and blocking autophagic flux, Oncotarget 7 (27) (2016) 42059–42070.
[14] J.I. Goldhaber, K.D. Philipson, Cardiac sodium-calcium exchange and efficient excitation-contraction coupling: implications for heart disease, Adv. Exp. Med. Biol. 961 (2013) 355–364.
[15] Y. Kurata, I. Hisatome, T. Shibamoto, Roles of sarcoplasmic reticulum Ca^{2+} cycling and Na^+/Ca^{2+} exchanger in sinoatrial node pacemaking: insights from bifurcation analysis of mathematical models, Am. J. Physiol. Heart Circ. Physiol. 302 (11) (2012) H2285–H2300.
[16] S. Hudecova, L. Lencesova, L. Csaderova, J. Sedlak, V. Bohacova, M. Laukova, O. Krizanova, Isoproterenol accelerates apoptosis through the over-expression of the sodium/calcium exchanger in HeLa cells, Gen. Physiol. Biophys. 32 (3) (2013) 311–323.
[17] F. Cuozzo, M. Raciti, L. Bertelli, R. Parente, L. Di Renzo, Pro-death and pro-survival properties of ouabain in U937 lymphoma derived cells, J. Exp. Clin. Cancer Res. 31 (2012) 95.
[18] T. Nashida, K. Takuma, S. Fukuda, T. Kawasaki, T. Takahashi, A. Baba, Y. Ago, T. Matsuda, The specific Na(+)/Ca(2+) exchange inhibitor SEA0400 prevents nitric oxide-induced cytotoxicity in SH-SY5Y cells, Neurochem. Int. 59 (1) (2011) 51–58.
[19] A. Soltysova, J. Breza, M. Takacova, J. Feruszova, S. Hudecova, B. Novotna, E. Rozborilova, S. Pastorekova, L. Kadasi, O. Krizanova, Deregulation of energetic metabolism in the clear cell renal cell carcinoma: a multiple pathway analysis based on microarray profiling, Int. J. Oncol. 47 (1) (2015) 287–295.
[20] B.A. Webb, M. Chimenti, M.P. Jacobson, D.L. Barber, Dysregulated pH: a perfect storm for cancer progression, Nat. Rev. Canc. 11 (9) (2011) 671–677.
[21] M. Pastorek, V. Simko, M. Takacova, M. Barathova, M. Bartosova, L. Hunakova, O. Sedlakova, S. Hudecova, O. Krizanova, F. Dequiedt, S. Pastorekova, J. Sedlak, Sulforaphane reduces molecular response to hypoxia in ovarian tumor cells independently of their resistance to chemotherapy, Int. J. Oncol. 47 (1) (2015) 51–60.
[22] B. Novotna, M. Takacova, S. Hudecova, L. Lencesova, J. Breza Jr., A. Misak, L. Csaderova, S. Pastorekova, O. Krizanova, J. Breza, Activation of the ER stress and calcium signaling in angiomyolipoma, Neoplasma 63 (5) (2016) 687–695.
[23] B. Chovancova, S. Hudecova, L. Lencesova, P. Babula, I. Rezuchova, A. Penesova, M. Grman, R. Moravcik, M. Zeman, O. Krizanova, Melatonin-induced changes in cytosolic calcium might be responsible for apoptosis induction in tumour cells, Cell. Physiol. Biochem. 44 (2) (2017) 763–777.
[24] O.H. Lowry, N.J. Rosebrough, A.L. Farr, R.J. Randall, Protein measurement with the Folin phenol reagent, J. Biol. Chem. 193 (1951) 265–275.
[25] L. Lencesova, S. Hudecova, L. Csaderova, J. Markova, A. Soltysova, M. Pastorek, J. Sedlak, M.E. Wood, M. Whiteman, K. Ondrias, O. Krizanova, Sulphide signalling potentiates apoptosis through the up-regulation of IP3 receptor types 1 and 2, Acta Physiol. (Oxf) 208 (4) (2013) 350–361.
[26] V. Sathish, P.F. Delmotte, M.A. Thompson, C.M. Pabelick, G.C. Sieck, Y.S. Prakash, Sodium-calcium exchange in intracellular calcium handling of human airway smooth muscle, PLoS One 6 (2011) e23662.
[27] S.S. Wang, Y.H. Chen, N. Chen, L.J. Wang, D.X. Chen, H.L. Weng, S. Dooley, H.G. Ding, Hydrogen sulfide promotes autophagy of hepatocellular carcinoma cells through the PI3K/Akt/mTOR signaling pathway, Cell Death Dis. 8 (3) (2017) e2688.
[28] J. Bae, M. Kumazoe, S. Yamashita, H. Tachibana, Hydrogen sulphide donors selectively potentiate a green tea polyphenol EGCG-induced apoptosis of multiple myeloma cells, Sci. Rep. 7 (1) (2017) 6665.
[29] P. De Cicco, E. Panza, C. Armogida, G. Ercolano, O. Taglialatela-Scafati, Y. Shokoohinia, R. Camerlingo, G. Pirozzi, V. Calderone, G. Cirino, A. Ianaro, The hydrogen sulfide releasing molecule acetyl deacylasadisulfide inhibits metastatic melanoma, Front. Pharmacol. 8 (2017) 65.
[30] A. Riemann, A. Ihling, B. Schneider, M. Gekle, O. Thews, Impact of extracellular acidosis on intracellular pH control and cell signaling in tumor cells, Adv. Exp. Med. Biol. 789 (2013) 221–228.
[31] P. Jóźwiak, A. Krześlak, L. Pomorski, A. Lipińska, Expression of hypoxia-related glucose transporters GLUT1 and GLUT3 in benign, malignant and non-neoplastic thyroid lesions, Mol. Med. Rep. 6 (2012) 601–606.
[32] M.R. Asgharzadeh, J. Barar, M.M. Pourseif, M. Eskandani, M. Jafari Niya, M.R. Mashayekhi, Y. Omidi, Molecular machineries of pH dysregulation in tumor microenvironment: potential targets for cancer therapy, Bioimpacts 7 (2) (2017) 115–133.
[33] M. Condrescu, J.P. Reeves, Inhibition of sodium-calcium exchange by KB-R7943: dodecylamine and sphingosine in transfected Chinese hamster ovary cells, Cell Calcium 47 (5) (2010) 404–411.
[34] I.N. Rich, D. Worthington-White, O.A. Garden, P. Musk, Apoptosis of leukemic cells accompanies reduction in intracellular pH after targeted inhibition of the Na^+/H^+exchanger, Blood 95 (4) (2000) 1427–1434.
[35] A. Porporato, P.R. Kramer, M. Cassiani, E. Daly, J. Mattingly, Local kinetic interpretation of entropy production through reversed diffusion, Phys. Rev. E - Stat. Nonlinear Soft Matter Phys. 84 (2011) 041142.
[36] H. Barriere, C. Poujeol, M. Tauc, J.M. Blasi, L. Counillon, P. Poujeol, CFTR modulates programmed cell death by decreasing intracellular pH in Chinese hamster lung fibroblasts, Am. J. Physiol. Cell Physiol. 281 (3) (2001) C810–C824.
[37] S.-N. Ge, M.-M. Zhao, D.-D. Wu, Y. Chen, Y. Wang, J.-H. Zhu, W.-J. Cai, Y.-Z. Zhu, Y.-C. Zhu, Hydrogen sulfide targets EGFR Cys797/Cys798 residues to induce Na(+)/K(+)-ATPase endocytosis and inhibition in renal tubular epithelial cells and increase sodium excretion in chronic salt-loaded rats, Antioxid. Redox Signal 21 (2014) 2061–2082.
[38] J. Xu, B. Ji, G. Wen, Y. Yang, H. Jin, X. Liu, R. Xie, W. Song, P. Song, H. Dong, B. Tuo, Na+/H+ exchanger 1, Na+/Ca2+ exchanger 1 and calmodulin complex regulates interleukin 6-mediated cellular behavior of human hepatocellular carcinoma, Carcinogenesis 37 (2016) 290–300.
[39] F. Yu, J. Zhao, C.S. Tang, B. Geng, Effect of synthesized GYY4137, a slowly releasing hydrogen sulfide donor, on cell viability and distribution of hydrogen sulfide in mice, Beijing Da Xue Xue Bao. Yi Xue Ban = J. Peking Univ. Health Sci. 42 (2010) 493–497.